Regular article

Nano-scale structural non-uniformities in gum like Ti-24Nb-4Zr-8Sn metastable β-Ti alloy

Qianglong Liang [a,b,c], Yufeng Zheng [b,c,*], Dong Wang [a,**], Yulin Hao [d], Rui Yang [d], Yunzhi Wang [b,c], Hamish L. Fraser [b,c]

[a] Center of Microstructure Science, Frontier Institute of Science and Technology, State Key Laboratory for Mechanical Behavior of Materials, Xi'an Jiaotong University, Xi'an, Shaanxi, China
[b] Center for the Accelerated Maturation of Materials (CAMM), The Ohio State University, Columbus, OH, USA
[c] Department of Materials Science and Engineering, The Ohio State University, Columbus, OH, USA
[d] Institute of Metal Research, Chinese Academy of Science, Shenyang, Liaoning, China

A R T I C L E   I N F O

A B S T R A C T

Phase instabilities in a recently developed gum like alloy, Ti-24Nb-4Zr-8Sn (Ti2448), were investigated using conventional and aberration-corrected scanning/transmission electron microscopy. Athermal ω (hexagonal) and O′ (orthorhombic) phases were found to be present in the alloy following solution treatment. A partial collapse of $\{111\}_\beta$ atom planes was observed in the ω phase, and a shuffle of every other $\{011\}_\beta$ atom planes along $\langle 01\bar{1}\rangle_\beta$ was observed in the O′ phase particle. The presence of both the ω and O′ phases in Ti2448 may influence the transition behavior under loading and may have significant impact on its mechanical properties.

© 2018 Acta Materialia Inc. Published by Elsevier Ltd. All rights reserved.

In recent years, a class of multifunctional metastable β-type Ti alloys, similar to gum metal [1], has attracted significant amount of attention due to its combination of attractive properties, such as superelasticity, high strength, great ductility, low modulus, invar effect (almost zero thermal expansion over a wide temperature range) and elinvar effect (temperature independence of elastic modulus) [1,2]. Much research has been conducted to explore the origin of such unique properties [2–13]. Although controversies still remain, it is generally accepted that these properties are related to martensitic transformations [2,3,7,8,12–15]. Tahara et al. have claimed that nanosized $\{110\}\langle 1\bar{1}0\rangle_\beta$ transverse lattice modulations induced by the local strain fields of randomly distributed oxygen atoms can suppress long-range (strain) order during the martensitic transformation in Ti-Nb-O alloy [9]. The superelasticity arises from the growth of the favorable variants of the nano-scale modulated domains and reorientation of the unfavorable variants [9]. Wang et al. claimed that nano-scale α″ martensitic domains exist in the conventional gum metal, Ti-23Nb-0.7Ta-2Zr-1.2O (at.%) [2], because of concentration inhomogeneities, which play an important

role in its superelasticity. Strong texture of these martensitic nanodomains develops after cold rolling, which leads to the invar anomaly and tunable thermal expansion [2].

As an important gum like Ti-alloy, Ti-24Nb-4Zr-8Sn (wt%, Ti2448) exhibits low Poisson's ratio, very high strength, superelasticity and tunable thermal expansion across a wide temperature range [16,17] and has attracted a great amount of interest [11,18,19]. However, the microstructural state in Ti2448 before deformation is still not fully characterized, which limits the understanding of this unique combination of properties. For example, it was shown by X-ray diffraction (XRD) and TEM characterization [10,16,18] that the solutionized and quenched Ti2448 alloy is a single β phase at room temperature. It has been claimed that the reversible mechanisms of local lattice distortions (nano-disturbance), dislocation loop and stress induced martensitic transformation in the initial β matrix induced by loading give rise to the nonlinear elastic deformation [16]. However, a recent synchrotron XRD study showed that the initial microstructure of Ti2448 before deformation is actually a mixture of B2 ordered regions with a distribution of nanoscale α″ martensitic domains (embryos) and bcc regions [19], all at nano-scale. Under loading, the α″ embryos grow, and the B2 and bcc regions transform to nanodomains of α″ and δ martensite, respectively, without the formation of long-range ordered martensitic domains [19]. More recently, by coupling 3-D atom probe tomography with synchrotron XRD, Wang et al. suggested that there exists a nanoscale concentration modulation in Ti2448 [11]. By phase field simulation, Zhu et al. [14]

* Correspondence to: Y. Zheng, CAMM, The Ohio State University, 1305 Kinnear Rd., Suite 100, Columbus, OH 43212-1177, USA.
** Correspondence to: D. Wang, Center of Microstructure Science, Frontier Institute of Science and Technology, State Key Laboratory for Mechanical Behavior of Materials, Xi'an Jiaotong University, Xi'an 710049, China.
E-mail addresses: zheng.510@osu.edu (Y. Zheng), wang_dong1223@xjtu.edu.cn (D. Wang).

were able to demonstrate that nanoscale concentration modulations within a parent phase matrix generated by spinodal decomposition could cause the stress induced martensitic transformation to occur continuously over a wide temperature range, which could explain the unique properties (e.g. superelasticity and tunable thermal expansion) across a wide temperature range observed in the experiment [14,17].

Because of these various possible explanations to account for the unique combinations of properties of gum like metals, it is essential to characterize microstructure accurately, including the types and nature of nano-domains present. Once characterized, the role that these nano-scale phases play in the various properties can be determined, leading to a fuller understanding of the deformation behavior of Ti2448. This paper describes the characterization of the microstructure in solutionized and quenched samples of this alloy.

The ingot of Ti2448 alloy (Ti-24Nb-4Zr-8Sn-0.2O wt%) with a diameter of 380 mm was fabricated in vacuum arc melter using a Ti-Sn master alloy with pure Ti, Nb and Zr (>99.9% purity) additions. The composition of the arc-melted alloy was measured as Ti-24.2Nb-3.96Zr-8.1Sn-0.2O by wet chemical and gas analysis. The ingot was then hot-forged at 1123 K to form round bars 25 mm in diameter, and they were cut into 50 mm × 50 mm × 12 mm small pieces, using a high-speed diamond saw, for further heat treatment. The cut samples were solutionized at 1173 K ($T_\beta \sim 1000$ K [20]) for 30 min in a tube furnace wrapped with pure titanium foil to decrease the oxidation and then quenched into cold water. Thin foils for TEM analysis were prepared

from the center part of the as-quenched samples, using a Dual-Beam Focused Ion Beam (DB-FIB) FEI Helios Nanolab 600 system, and the ion beam damage on the foil surfaces resulting from the DB-FIB was minimized using low voltage Ar^+ ion milling in a Fischione Nanomill™ Model 1040. Selected area diffraction (SAD) pattern and dark field images were recorded on a FEI Tecnai30 transmission electron microscope operating at 300 kV, and high angle annular dark field-scanning transmission electron microscopy (HAADF-STEM) was carried out using a probe-corrected FEI Titan3™ 80–300 operated at 300 kV, using a convergence semi-angle of 12 mrad and a collection semi-angle of 44 mrad, with an incident beam dwell-time of 4 μs/px and a beam current of ≈100 pA. Line profiles in TEM diffractions were evaluated using ImageJ.

The SAD patterns recorded from $[011]_\beta$, $[113]_\beta$, and $[100]_\beta$ zone axes in the as-quenched Ti2448 are shown in Fig. 1(a–c). In Fig. 1(a), ω reflections located at 1/3 and 2/3$(2\bar{1}1)_\beta$ in the $[011]_\beta$ zone axis can be clearly observed together with the O′ phase reflections located at 1/2 $(2\bar{1}1)_\beta$, highlighted separately using the dashed green circles and the yellow circle, respectively. The presence of ω and O′ reflections can be validated by the intensity profile drawn along the dashed yellow line, from the transmitted spot to the $(2\bar{1}1)_\beta$ reflection shown in the inset. Thus, three intensity maxima are observed: the highest corresponds to the O′ phase and the other two originating from the ω phase. The corresponding dark field image selecting the ω reflections and O′ reflection in the red circle is shown in Fig. 1(d). A large number density of nano-scale
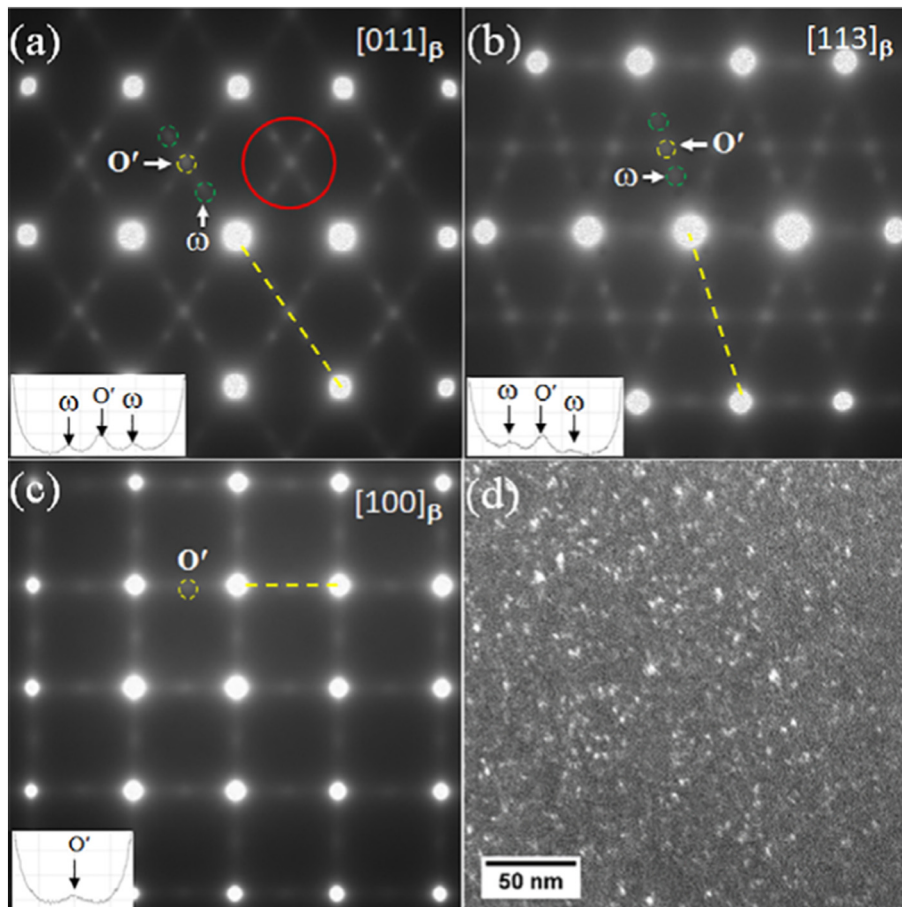

Fig. 1. SAD patterns and dark field image recorded from the as-quenched Ti2448: (a–b) SAD pattern from $[011]_\beta$ and $[113]_\beta$ zone axes showing the co-existence of ω reflection (highlighted by green color circle) and O′ reflection (highlighted by yellow color circle); inset line intensity profile along the yellow dashed line showing the maxima at 1/3 and 2/3 $\{112\}_\beta$ and 1/2 $\{112\}_\beta$ belonging to ω phase and O′ phase respectively; (c) SAD pattern from $[100]_\beta$ zone axis showing the presence of O′ reflection (highlighted by yellow color circle); inset line intensity profile along the yellow dashed line showing the maxima at 1/2 $\{013\}_\beta$ belonging to O′ phase; (d) corresponding dark field image from (a) by selecting the ω and O′ reflections in the red color circle showing the presence of athermal ω phase and O′ phase domains of approximately 3–5 nm diameter.